IMPREGNATION OF β-TRICALCIUM PHOSPHATE ROBOCAST SCAFFOLDS BY *IN-SITU* POLYMERIZATION

Francisco J. Martínez-Vázquez, Fidel H. Perera, Inge van der Meulen[1], Andreas Heise[1], Antonia Pajares, Pedro Miranda[*]

Departamento de Ingeniería Mecánica, Energética y de los Materiales. Universidad de Extremadura.
Avda de Elvas s/n. 06006 Badajoz, Spain

[1] Laboratory of Polymer Chemistry, Eindhoven University of Technology, P.O. Box 513, 5600 MB Eindhoven, The Netherlands

June 21, 2012

---

[*] Corresponding author. Email: pmiranda@unex.es

ABSTRACT

Ring-opening polymerization of ε-caprolactone (ε-CL) and L-lactide (LLA) was performed to impregnate β-tricalcium phosphate (β-TCP) scaffolds fabricated by robocasting. Concentrated colloidal inks prepared from β-TCP commercial powders were used to fabricate porous structures consisting of a 3-D mesh of interpenetrating rods. ε-CL and LLA were *in-situ* polymerized within the ceramic structure by using a lipase and stannous octanoate, respectively, as a catalysts. The results show that both the macropores inside the ceramic mesh and the micropores within the ceramic rods are full of polymer in either case. The mechanical properties of scaffolds impregnated by *in situ* polymerization (ISP) are significantly increased over those of the bare structures, exhibiting similar values than those obtained by other, more aggressive, impregnation methods such as melt-immersion (MI). ISP using enzymatic catalysts requires a reduced processing temperature which could facilitate the incorporation of growth factors and other drugs into the polymer composition, thus enhancing the bioactivity of the composite scaffold. The implications of these results for the optimization of the mechanical and biological performance of scaffolds for bone tissue engineering applications are discussed.

Key Words: Ring Opening Polymerization, Polymer impregnation, Robocasting, Scaffolds, Mechanical properties.

1. INTRODUCTION

The development of synthetic biodegradable scaffolds suitable for bone substitution and regeneration in load bearing regions of the skeleton remains a scientific challenge. Biodegradable scaffolds should provide structural support for cell growth during regeneration of the tissue, and then be progressively resorbed and replaced by the newly-formed bone. Moreover, when load-bearing applications are targeted, the scaffold should also be able to maintain mechanical integrity during the tissue regeneration process until the newly-formed bone takes over.

Required cell support features can be achieved by fabricating an appropriate porous structure from an osteoconductive material. Among the different material options, tricalcium phosphate (TCP, $Ca_3(PO_4)_2$) bioceramics are attractive since they exhibit a higher biodegradability (higher resorption rate) than other appealing candidates such as hydroxyapatite (HA, $Ca_{10}(PO4)_6(OH)_2$) [1]. The interconnected pore structure necessary for cell proliferation and diffusion of nutrients can be well controlled by using a solid freeform fabrication (SFF) technique such as robocasting (also known as micro-robotic deposition) for fabricating the scaffold. The layer-by-layer fabrication scheme employed by these techniques allow one to build structures with customized and complex 3D shapes from a computer-aided design (CAD) model, thus producing porous structures with controlled mechanical behavior, permeability, and diffusion properties and with an external shape matching the damaged tissue site. In particular, robocasting consists of the robotic deposition of highly concentrated colloidal suspensions (inks) with minimal organic content capable of fully supporting their own weight during assembly [2, 3]. Thus, a 3-D mesh of interpenetrating rods is built

layer-wise by extrusion of the inks through the deposition nozzle following the pattern specified in the CAD model.

However, despite their improved pore architecture, even robocast bioceramic scaffolds lack sufficient mechanical strength and toughness to be suitable for load-bearing applications [4]. One alternative to overcome this hurdle would be to fabricate robocast composite structures using polymeric inks reinforced with bioceramic particles [5] but this comes at the expense of a reduced elastic modulus. Alternatively, one can add an appropriate biodegradable polymeric phase to the bioceramic structure in order to develop a composite material with enhanced toughness [6, 7] and strength [8] and without jeopardizing the modulus. In previous work, this idea was successfully tested on robocast scaffolds which were impregnated by immersion in commercial polylactic acid (PLA) and polycaprolactone (PCL) polymer melts [9].

Nonetheless, the aforementioned impregnation method is not believed to be the best alternative for the incorporation of the polymeric phase to the scaffold. Indeed, an additional advantage of incorporating a polymeric material would be the possibility to use it as a vehicle for biomolecules (growth factors, antibiotics, anti-inflammatory drugs, etc.), for controlled delivery. However, incorporation of such biomolecules does not allow for the extreme temperatures [10], far above 200 °C, needed for the melt-immersion (MI) impregnation method. Instead, biomolecules are usually incorporated to biodegradable polymers by physisorption, chemisorption or grafting and coatings are usually produced by immersion of the substrate in polymer solutions [11]. However, dip-coating process does not allow a full impregnation [6, 7] of the porous structures due to the inability of the polymer to fill the voids produced by the evaporation of the solvent. Thus, in this work a different process for a complete impregnation of porous ceramic scaffolds with biodegradable polymers is optimized

and tested. The method consists of the *in situ* polymerization (ISP) of the corresponding monomers or dimers — ε-caprolactone (ε-CL) and L-lactide (LLA) are used here — within the ceramic structure. A similar procedure has been successfully applied for the infiltration of conventional porous scaffolds by other authors[12-16], but this is the first work in which this infiltration technique is compared to other methods in a controlled scaffold geometry fabricated by a solid freeform fabrication technique. Fully impregnated TCP structures are thus fabricated by ISP and their microstructures and mechanical properties are analyzed and compared to those of PLA-TCP and PCL-TCP composites fabricated by the MI method. Nonetheless, in this regard, it is worth indicating that the processing conditions and the polymers used in this study are selected with a focus on optimizing the mechanical performance of ISP composites and comparing it with those fabricated by MI [9], and not so much at optimizing the biological performance. Fully impregnated scaffolds could generate the porosity necessary for bone ingrowth *in situ* upon implantation, provided an appropriate polymer bioerosion behavior. For the materials selected here this would not be the case, since both PLA and PCL are not fast-resorbing polymers and they degrade in bulk rather than in surface. In any case, these dense composites could find application as temporary orthopedic fixation devices (plates, pins, screws, etc.), since they would exhibit a better performance in terms of elastic, osteointegration and biodegradation properties than the pure polymers [17-19]. The results of this work supply useful information for the development of novel composite materials orthopedic applications, with enhanced mechanical and biological performance.

2. EXPERIMENTAL PROCEDURE

2.1. Robocast scaffolds preparation

Commercially available Ca-deficient powder (21218, Sigma Aldrich), pre-calcined at 1300 °C (dwell time: 10 min, heating/cooling rate: 10 °C/min) to obtain a final 84 wt% β-TCP/16 wt% α-calcium pyrophosphate (CPP) composition [20] and attritor milled to around 1 μm particle size, was used to prepare inks for robocasting with a final solid content of 45 vol%, following a procedure similar to that of previous works [2, 4]. First, a stable suspension was prepared by dissolving 1.5 wt% (relative to powder content) Darvan® C dispersant (R.T. Vanderbilt, Norwalk, CT) in distilled water, and a gradual addition of the β-TCP powder. An appropriate amount (7 mg/ml of liquid in the final suspension) of predissolved hydroxypropyl methylcellulose (Methocel F4M, Dow Chemical Company, Midland, MI) was then added to the mixture to increase viscosity. Subsequently, the ink was gellified by adding 2 vol% (relative to liquid content) of polyethylenimine (PEI) as flocculant. After each addition, the mixture was placed in a planetary centrifugal mixer (ARE-250, Thinky Corp., Tokyo, Japan) for a few minutes to improve its homogeneity and stability.

Three-dimensional β-TCP scaffolds consisting of a mesh of ceramic rods were constructed layer by layer via direct-write assembly of the ink using a robotic deposition device (3-D Inks, Stillwater, OK). The printing syringe was partially filled with the ink and placed on the 3-axis motion stage, controlled independently by a computer-aided direct-write program (Robocad 3.0, 3-D Inks, Stillwater, OK). The ink was deposited through conical polymeric deposition nozzles (EFD Inc., East Providence, RI) with a tip diameter $d = 250$ μm, at a printing speed of 30 mm/s. Each layer in the computer 3D model of the structure consisted of parallel rods with a spacing from center to center $s = 500$ μm. Rods in adjacent layers are perpendicularly oriented and the spacing between layers was set to $h = 175$ μm. The external dimensions of the scaffolds were set at about 17 mm × 17 mm × 10 mm so that a total of 60 layers were deposited. The

deposition was done in a paraffin oil bath to prevent non-uniform drying during assembly.

The samples were extracted from the bath and dried in air at room temperature for at least 24 hours, and then at 400 °C (1 °C/min heating rate) for 1 hour to remove organics. They were finally sintered at 1200 °C (heating rate 3 °C/min) for 2 hours (cooling rate: 10 °C/min), which are the optimal sintering conditions for this particular type of powders [20].

Density of the sintered scaffolds was measured as total weight divided by external volume. Total porosity was determined from these measurements by considering 3.07 g/cm^3 as theoretical density for the TCP material, and the percentage of closed porosity was measured by He-pycnometry.

2.2. Polymer infiltration process

Some composites were fabricated by MI impregnation as a benchmark for comparison, using a procedure described in previous work [9]. Briefly, commercial pellets of PLA (Natureworks, Minnetonka, MN) or PCL (Purac, Barcelona, Spain) were melted at 227 °C and 220 °C, respectively. TCP scaffolds were then immersed in the melts, soaked for 2h, and cooled to room temperature. Commercial, off-the-shelf, polymers are the logical choice for usage in a MI process since thus the hurdles of controlling the polymerization process are avoided, being precisely its simplicity one of the most appealing features for the industrial application of this method. Also, since commercial polymers usually possess higher molecular weight and lower polydispersity than those typically obtained in laboratory polymerization processes, they constitute, in principle, the most stringent benchmark for the proposed ISP method.

For the in-situ polymerizations proposed in this work as an improved alternative process of impregnation, enzymatic ring-opening polymerization [21] was considered to be the optimal route to reduce the impregnation temperature. Unfortunately, LLA dimer is solid and, since solventless synthesis is required to produce a fully dense structure, in that case the temperature could not be reduced below the melting temperature of the dimer (116-119 °C), which prevented the use of enzymes. Instead, stannous octanoate catalyst and a reaction temperature of 140 °C were selected for the polymerization of LLA.

Ring-opening polymerization of ε-CL and LLA were carried out on selected scaffolds to develop a polymeric continuous phase within the ceramic structure. Commercial ε-CL and LLA were obtained from Aldrich Chemical Co, but while LLA was used without further purification, ε-CL was first dried over calcium hydride and then distilled under reduced pressure. Novozym 435 — *Candida antarctica* Lipase B immobilized on cross-linked polymethylmethacrylate beads — was purchased from Novozymes A/S and dried following a procedure described elsewhere [22]. Stannous octanoate was purchased from Aldrich Chemical Co. and distilled under reduced pressure.

For the impregnation of scaffolds with PCL, Novozym 435 (120 mg) and the selected TCP scaffold were dried in the reaction flask over molecular sieves at 40 °C overnight in a vacuum oven. After drying, the oven was opened under nitrogen flow. The flask, containing Novozym 435 and the ceramic sample, was stoppered with a rubber septum and the monomer (2 mL, enough to cover the scaffold) was added by syringe through the septum under nitrogen atmosphere. The mix was then placed in an oil bath at 60 °C for 72 hours — this temperature has been shown to produce polymers with maximal molecular weight [23] . Initial water content just after starting strirring the

reaction mixture was measured by Karl Fischer Coulometry (DL32 Coulometer, Mettler Toledo), using Apura CombiColoumat fritless (Merck) as electrolyte. The total water content (wt/wt) in all reactions was below 0.003%.

For the impregnation with PLA, lactide and the selected scaffolds were dried in the reaction flask over molecular sieves at 40 °C overnight in a vacuum oven. Separate stock solutions of catalyst and initiator were prepared. After drying, the oven was opened under nitrogen flow and the flask was placed in an oil bath at 140 °C. When the dimer was melted, stannous octoate (0.03 wt %) and previously destilled benzyl alcohol (Sigma Aldrich; 800:1 molar ratio) were added to the flask by syringe trough the septum under nitrogen atmosphere.

In both cases, the reaction was stopped after 72 hours and the ceramic structure was removed from the reaction flask and the spare polymer was used for molecular weight (M_n) and polydispersity index (PDI) evaluation — after verifying that there was little difference with the polymer inside the scaffold (recovered by dissolving the polymer within the structure in THF prior to measurements). Both magnitudes were measured with size exclusion chromatography (SEC), based on polystyrene standards (Polymer Laboratories, from M_p = 580 g/mol up to $M_p = 7.1\times10^6$ g/mol). For PLA samples, high temperature SEC was performed on a Polymer Laboratories PLXT-20 Rapid GPC Polymer Analysis System (including pump, refractive index detector and viscosity detector) at 160 °C with 3 PLgel Olexis (300 × 7.5 mm, Polymer Laboratories) columns in series. 1,2,4-Trichlorobenzene was used as eluent at a flow rate of 1 mL/min. A Polymer Laboratories PL XT-220 robotic sample handling system was used as autosampler. SEC on PCL samples was performed on a Waters Alliance system equipped with a Waters 2695 separation module, a Waters 2414 refractive index detector (40 °C), a Waters 2487 dual absorbance detector and a Polymer Laboratories

PLgel guard column followed by 2 PLgel 5mm Mixed-C columns in series at 40 °C. Tetrahydrofuran (THF, Biosolve), stabilized with BHT, was used as eluent at a flow rate of 1 mL/min. All samples were filtered through a 0.2 μm PTFE filter (13 mm, PP housing, Alltech) before analysis.

PLA polymers samples obtained from the periphery of both MI and ISP scaffolds were also characterized by XRD to analyze their crystallinity. The XRD data were collected in step-scanning mode (step width 0.02° 2θ, angular interval 5-60° 2θ, and count time 0.1 s/step) using a high-resolution laboratory diffractometer (D8 Advance, Bruker AXS, Karlsruhe, Germany) equipped with a primary monochromator that provides pure $CuK_{\alpha 1}$ radiation (λ = 1.54183 Å) and a linear ultra-fast detector.

2.3. Mechanical and microstructural characterization

Rectangular parallelepiped specimens with dimensions of around 3 × 3 × 6 mm were cut (Accutom-50, Struers, Germany), perpendicularly to rod axes, from both the as-sintered and the infiltrated structures by both ISP and MI methods for scanning electron microscopy (SEM) observation and mechanical characterization by uniaxial compression tests. SEM microscopy (S-3600N, Hitachi Ltd., Tokyo, Japan) using both secondary and backscattered electrons was made on gold-coated samples. Dimensional measurements were made by routine image analysis (AnalySIS1, Olympus Soft Imaging Solutions, GmbH, Germany). Fracture surfaces obtained after 4-point bending tests performed at a crosshead speed of 15 mm/min on samples of 27 × 4 × 2 mm were also SEM-imaged to further characterize the materials.

The uniaxial tests were carried out on a universal testing machine (AG-IS10kN, Shimadzu Corp., Kyoto, Japan), in air, at a constant crosshead speed of 0.6 mm/min.

Tests were performed along the sample height, in the direction perpendicular to the printing plane (i.e., orthogonal to the rod axes), which has been shown to be a weak direction in these ceramic structures [4, 24]. Engineering stress-strain curves were calculated through normalization of captured load *vs* displacement data using the initial external dimensions of each sample. A total of 25 samples were tested in each case in order to get statistically reliable values. The compressive strength of the structure was estimated as the maximum stress applied in each test. Weibull statistics [25] were used to analyze the resulting strength data. Toughness was estimated as the strain energy density [7] at two strain values: strain at compressive strength (G_{max}) and 10% strain ($G_{0.1}$), from the corresponding integrals of the nominal stress–strain curve. When necessary to elucidate the significance of observed differences, ANOVA tests at 95% confidence level and Tukey's post-hoc tests were used.

Intrinsic mechanical properties of the individual materials were also evaluated. Instrumented indentation (Nanotest, Micro Materials Ltd., Wrexham, U.K.) was used to determine their elastic modulus and hardness. The indentation tests were performed using a diamond Berkovich indenter on polished sections of the infiltrated scaffolds (to 1 μm finish). Single indentations of about 1 μm depth were placed at the center of polymer filled areas. The indent size (~ 7 μm) is small enough to avoid the influence of the nearby β-TCP rod surfaces. Properties of bare TCP rods were determined Single indentations of about 40 μm size placed at the center of TCP rods, so that they were large enough compared to grain size to provide meaningful information about the mechanical properties of the rods (and not of individual grains) but small enough to avoid the influence of the free surfaces of the rods.

3. RESULTS

Figure 1 shows SEM micrographs of representative cut specimens of the β-TCP robocast scaffolds before impregnation. Both the macroscopic, pre-designed porosity (Fig. 1a and b) and the internal rod porosity (Fig. 1c) are apparent. For the sake of simplicity, we will from now on refer to the former as macroporosity and to the latter as microporosity. SEM images as that shown in Fig. 1b allowed the average dimensions of the bioceramic structure to be measured as: rod diameter, $d = 215 \pm 8$ μm, center-to-center rod spacing, $s = 436 \pm 10$ μm, and center-to-center layer spacing, $h = 162 \pm 5$ μm. Density measurements determined a total porosity of ~68% in the bare β-TCP scaffolds of which ~64% was open porosity, and thus accessible to the polymer.

Figure 2 shows SEM micrographs of representative specimens of the β-TCP robocast scaffolds after impregnation with PCL (Figs. 2a and 2c) and PLA (Figs. 2b and d) by ISP. These micrographs confirm ISP as an excellent impregnation technique since they show that the polymers not only completely fill the macropores (Fig. 2a and b) but even penetrate into the rods' microporosity, as shown in the backscattered electron micrographs of fractured rod surfaces of Figs. 2c and 2d. The degree of infiltration is similar to that observed in scaffolds impregnated by MI method (not shown) [9].

The results of the characterization of the individual materials are summarized in Table 1. These results show that while the laboratory process of ISP yields polymers with somewhat lower molecular weights and larger PDI than their commercial counterparts used for MI, their mechanical performance in terms of modulus and hardness is, to all purposes, unchanged.

Regarding the mechanical characterization of the fabricated scaffolds, Fig. 3 shows representative nominal stress-strain curves for uniaxial compressive tests

performed on the bare β-TCP scaffolds and structures impregnated with PLA (labeled TCP-PLA) and PCL (TCP-PCL). Curves for scaffolds impregnated by MI are included for comparison together with those corresponding to ISP infiltrations. It should be noted that curves for MI-PCL impregnated structures do not exhibit a maximum, but a drastic slope reduction is observed after a certain applied stress. Since this transition is attributed to the fracture of the ceramic skeleton, the transition stress, calculated from the intersection of the linear best fits to data before and after the transition, was taken as the compressive strength of the composite structure. A significant (at 95% confidence level) improvement in the compressive strength of the TCP scaffolds is apparent upon infiltration of either PCL or, especially, PLA. No significant dependence on the impregnation method (MI *vs*. ISP) is observed. Moreover, the continuous polymeric phase provides the structure with a greatly enhanced toughness, as evidenced by the capacity of the samples to retain mechanical integrity even after very large deformations (see inset in Fig. 3). However, strain energy density does seem to depend on the impregnation method, as evidenced by the variations in the area underneath the curves, although the effect seems to be reversed depending on the polymer: while ISP improves toughness of the PLA-TCP structures over MI technique, it reduces that of PCL-TCP scaffolds.

The strengthening effect of polymer infiltration can be observed more clearly in the Weibull plots of Fig. 4. This plot shows the failure probability as a function of applied compressive stress for bare β-TCP scaffolds (open circles) and structures impregnated with PLA (squares) and PCL (triangles) either by ISP (dark-filled symbols) or MI (light-filled symbols). The straight lines are the best fits using the Weibull probability function [25]:

$$P = 1 - \exp[-(\sigma/\sigma_0)^m] \quad (1)$$

with P being the failure probability, and where the Weibull modulus, m, and central value, σ_0, are adjustable parameters whose values are summarized in Table 2. In particular, it is clear that the average compressive strength (or the central value) of the scaffolds is nearly tripled upon impregnation with PCL and increased by a factor of 10-11 in the case of PLA infiltration. No significant differences on the strength central value are observed between the impregnation methods, although the data scatter is relatively larger for ISP impregnated structures. This reduction in the reliability of the impregnated structures is more significant in the case of PCL where the Weibull modulus is reduced from $m = 11.7 \pm 0.6$ in MI impregnated structures to $m = 5.0 \pm 0.3$ in ISP composites.

For the quantification of the toughening effect of polymer infiltration, Fig. 5 (and also Table 2), shows the strain energy density at two strain values: strain at compressive strength (G_{max}) and 10% strain ($G_{0.1}$). Independently of the strain considered, full impregnation of the scaffolds increases the toughness by more than one order of magnitude. It is also evident that PLA is a more effective infiltrate than PCL for increasing the strain energy density in compression, regardless the impregnation method. This does not mean that strain energy density is independent of impregnation method since, as already mentioned, ISP improves toughness of the PLA-TCP structures over MI technique, and reduces that of PCL-TCP scaffolds, although only after the failure of the ceramic skeleton (i.e. reduces $G_{0.1}$ but not G_{max}).

4. DISCUSSION

The results of Figure 2-5 and Table 1-2 demonstrate that ISP is a suitable polymer impregnation method for robocast scaffolds, producing a good infiltration of the polymers into the scaffolds' pores (both macropores and micropores, see Fig. 2) at temperatures much lower than in the MI technique and without degrading the impregnated scaffolds' mechanical performance significatively. This reduction in temperature, especially in the case of PCL where enzymatic ring-opening polymerization could be used, was down to temperatures at which incorporation of bioactive molecules (such as growth factors, antibiotics and anti-inflammatory drugs etc.) in the biopolymer should be possible. Indeed, although the polymerization conditions used here (60 ºC, 72 h) might be a little harsh for most biomolecules, those conditions — selected in order to maximize the molecular weight of the polymer, and hence its mechanical properties — could be adjusted to preserve the integrity of the target biomolecule.

Concerning the performance of the impregnated scaffolds, the results in Figure 3 and 4 reveal that the average compressive strength of the composite structures is, to all purposes, the same regardless of the impregnation method (ISP or MI). The only observable difference is a reduction in the reliability (indicated by a decrease in the slope of the corresponding curves in Fig. 4) in ISP-impregnated structures, which hints at a slightly lower uniformity on the degree of infiltration.

Conversely, there is a significant (at 95% confidence level) effect of the polymer infiltration method on the strain energy density of the impregnated scaffolds, as shown in Figures 3 and 5. This is undoubtedly related to changes in the intrinsic toughness of the polymers. As already mentioned in the preceding section, the effect is opposite

depending on the polymer: ISP process seems to improve the toughness of PLA over MI technique, while it reduces that of PCL. The latter effect can be easily explained based on the differences in the molecular weight of PCL polymers resulting from both methods, the lower M_n of ISP-PCL translates into a reduced elongation at fracture [26], which explains the reduced strain energy density ($G_{0.1}$) in the corresponding impregnated scaffolds (Fig. 5, Table 2). Evidence of this reduction in the elongation at fracture of PCL produced by ISP is shown in the SEM micrographs of Figure 6, obtained in samples fractured by bending. Indeed, the ISP-PCL of Figure 6a and c exhibit a very irregular fracture surface typical of semicrystalline polymers, but there is no sign of the overstretched polymer filaments that are ubiquitous in the fracture surfaces of PCL-TCP structures fabricated by MI impregnation (Fig. 6b and d).

On the contrary, in the case of PLA, the molecular weight differences cannot explain the experimental results since the ISP-PLA is found to be tougher than MI-PLA, despite its lower M_n value. It is not so surprising that molecular weight should be less relevant in the case of PLA since this polymer at room temperature is in its glassy mechanical regime (unlike PCL which is in its rubbery regime). However the fracture surfaces of PLA-TCP composites obtained by bending confirm that the ISP process produces a tougher PLA polymer. As shown in Fig. 7, the ISP-PLA exhibits a very irregular fracture (Fig. 7a and c), while MI-PLA shows virtually smooth fracture surfaces (Fig. 7b and d). This reflects the very different degrees of crystallinity of both polymers: while ISP-PLA is highly crystalline, the MI-PLA is practically amorphous, as confirmed by XRD analysis (Fig. 8).

In any case, regardless of the impregnation method used, this study corroborates the results obtained in previous work [9] which showed a substantial improvement on the mechanical performance of the TCP scaffolds, both in terms of strength and toughness,

upon polymer infiltration (Figs. 3-5). In particular, the present results show that the compressive strength of the TCP scaffolds is increased approximately by a factor of 3 upon impregnation with PCL and by a factor of 11 in the case of PLA infiltration (Fig. 4 and Table 2). Moreover, the strain energy density in compression is boosted by more than one order of magnitude in our fully-impregnated structures (Fig. 5, Table 2), an enhancement far superior to those reported in partially impregnated scaffolds by other authors (< 50%) [7], although obviously the latter have the advantage of preserving an interconnected porosity for bone ingrowth.

The toughening obtained is inherent to the introduction of a continuous tougher polymeric phase which holds the structure together even after the ceramic skeleton fails. The enhanced performance of PLA over PCL in terms of strain energy density in compression is related to its superior strength which compensates for its inferior ductility [9]. On the other hand, the strengthening is due to a dual effect of the polymer infiltrate. Firstly the polymer within the micropores acts as a healing agent of pre-existing flaws in the ceramic scaffold surfaces, bonding the defect walls together and thereby increasing the stress needed to propagate a crack from them. Secondly, the polymer on the macropores sustains part of the applied load in the hybrid structures —a larger part as the polymer stiffness increases— thus reducing the tensile stresses acting on the ceramic rods, as demonstrated by finite element analysis in a previous work [9]. Consequently, this stress reduction mechanism explains why PLA-impregnated scaffolds exhibit strengths substantially higher (~ 4 times) than those of PCL-TCP hybrid scaffolds since, according to previous results, the stress reduction is negligible in the latter case due to the low elastic modulus of PCL [9]. Accordingly, the dominant strengthening effect in PCL-TCP structures is defect-healing, a surface strengthening effect that should be possible to preserve by only coating the rods with the polymer,

opening a way to produce robocast scaffolds with enhanced compressive strength but preserving the macroscopic pre-designed pore architecture to induce bone in-growth. Studies are currently under way to verify this assertion.

Nonetheless, the use of fully-impregnated composite scaffolds similar to those developed here by ISP could be of interest in itself. They will exhibit a better performance in terms of elastic, osteointegration and biodegradation properties than the pure polymers [17-19], which will make them suitable candidates for use in temporary orthopedic fixation devices. Moreover, these dense hybrid materials could have mechanical properties superior to those of simply coated structures due to stress shielding, provided the infiltrating polymer was sufficiently stiff. Indeed, as shown in Figure 9 where the different mechanical parameters evaluated (σ_C and $G_{0.1}$) for the hybrid structures are compared to natural bone properties [27, 28] and data from other authors [7], PLA-TCP structures reach values far superior to those reported in coated structures (despite the lower initial values of the bare structure) and well within the range of cortical bone properties, both in terms of strength and toughness. This suggests that there might be a potential for the application of this particular type of hybrid structures in load bearing applications, especially if the geometry and initial properties of the bare structure were optimized.

Of course, before the aforementioned potential applications can be realized further studies would be needed to assess the non-toxicity of these hybrid materials — concerns might be raised by the fact that the catalysts remain embedded within the polymer in ISP —, and to analyze how these materials would integrate with surrounding bone tissue.

Regarding this latter issue, it is worth mentioning that if the bioerosion rate of the polymer infiltrates is tuned to be higher than that of the calcium phosphate skeleton, the porosity necessary for bone ingrowth could be progressively generated *in situ* upon implantation, provided that surface bioerosion is the polymer degradation mechanism. During the resorption process, more and more of the load would be transferred from the initially strong hybrid material onto the newly-formed bone, which would enhance the regeneration process and preserve the mechanical integrity of the implant-tissue system until full resorption of the scaffold materials. Obviously, the scientific challenge would be to determine the appropriate scaffold's materials and microstructure to achieve that.

In this regard, ISP impregnation by enzymatic ring-opening polymerization (as used here for ε-CL) could be considered the most appropriate fabrication method for the dense hybrid scaffolds fabricated since, as already mentioned, its lower processing temperature will enable the modification of the polymeric phase to act as a delivery system of biomolecules capable of modulating the whole regeneration process. Effectively, this method presents the advantages that the polymer phase is added to the ceramic structure by synthesis, so that the temperature reached during the polymer deposition (≤ 60 °C) is lower than that used in MI impregnation (> 200 °C), potentially avoiding the thermal degradation of the biomolecules it will carry and deliver. Moreover, the use of a non-toxic enzymatic catalyst does not jeopardize the biocompatibility of the polymer, and provides additional advantages over conventional polymerization methods. These include (a) mild reaction conditions, i.e., temperature, pH, and absence of organic solvents, (b) high enantio- and regioselectivity, (c) require only low amounts of enzyme to achieve a good level of polymerization within a reasonable time scale[23, 29]. Obviously, studies will have to be devoted to optimizing the

actual reaction conditions necessary to preserve the integrity of each target biomolecule to be incorporated into the corresponding polymer infiltrate.

5. **CONCLUSIONS**

The results of this study confirm that dense hybrid ceramic/polymer bioactive materials are promising candidates for bone substitution and regeneration since they exhibit enhanced mechanical performance both in terms of strength and toughness over bare bioceramic structures. *In situ* polymerization (ISP) using either enzymatic (for ε-CL) or conventional (for LLA) catalysts has been shown in this work to be a successful and favorable path to impregnate robocast scaffolds by organic solventless synthesis. Indeed, full impregnation of the initial scaffold open porosity was obtained at milder processing temperatures compared to other impregnation methods such as melt immersion (MI). Enzymatic ring-opening polymerization — achieved here for ε-CL at 60 °C, 72h — can reduce the temperature to levels that could allow the incorporation of non-degraded biomolecules to the polymer composition, to act as a vehicle for controlled drug delivery, without degrading the mechanical performance of the composites. For this purpose polymerization conditions (temperature, time, catalyst, etc.) might have to be adjusted to preserve the integrity of the target biomolecule, possibly at the expense of a reduced molecular weight of the resulting polymer. Besides, a careful selection of the material comprising these hybrid ceramic/polymer structures might produce bioactive materials with density, toughness and strength similar to human bone that could also induce full regeneration of large bone lesions, through the generation of porosity *in situ* during their biodegradation. The realization of such

optimal biomaterials remains a scientific challenge, although the results of this study constitute a significant step in the right direction.

ACKNOWLEDGEMENTS

The authors want to thank Prof. Cor E. Koning for useful discussions and for enabling the stay of F. J. Martinez-Vazquez at the Laboratory of Polymer Chemistry, Eindhoven University of Technology to perform this study. This work was supported by the Ministerio de Ciencia e Innovación (PET2008_0168_02), Junta de Extremadura (IB10006) and FEDER funds.

FIGURE CAPTIONS

1. SEM micrographs of representative cut specimens of the β-TCP robocast scaffolds before impregnation. Both the macroscopic, pre-designed porosity (a, b) and the internal rod porosity (c) are shown.

2. SEM micrographs of representative specimens of robocast β-TCP scaffolds after impregnation with PCL (a, c) and PLA (b, d) by ISP: low magnification secondary electron images (a, b), and backscattered electron micrographs of fractured rod surfaces (c, d). The polymers (darker regions) fill both the macro- and open microporosity within the ceramic scaffold (lighter regions).

3. Representative nominal stress-strain curves obtained during uniaxial compression tests performed on robocast β-TCP scaffolds along the direction orthogonal to the rod layers, before (black lines) and after impregnation with PCL or PLA (as indicated) by either ISP (solid lines) or MI (dashed lines) techniques, as indicated. Inset shows an image of representative compression specimens before and after the tests.

4. Weibull compressive strength plot (i.e., failure probability *vs.* applied stress) for bare β-TCP scaffolds (open circles), and for PCL-TCP (squares) and PLA-TCP (triangles) hybrid structures, fabricated by either ISP (lighter color) or MI (darker color). The straight lines are linear fits to data using a Weibull probability function.

5. Strain energy densities obtained at two strain values: strain at compressive strength (G_{max}, lighter color) and 10% strain ($G_{0.1}$, darker color). Results are

shown for bare β-TCP scaffolds, and for PCL-TCP and PLA-TCP hybrid structures fabricated by either ISP or MI (as indicated), with standard deviations as error bars.

6. SEM backscattered electron micrographs of fracture surfaces on PCL-TCP hybrid structures fabricated by ISP (a, c) and MI (b, d). Darker regions represent PCL and lighter areas β-TCP. ISP samples exhibit irregular fracture surfaces but without the overstretched polymer filaments evident in MI samples.

7. SEM backscattered electron micrographs of fracture surfaces on PLA-TCP hybrid structures fabricated by ISP (a, c) and MI (b, d). Darker regions represent PLA and lighter areas β-TCP. ISP samples exhibit more irregular fracture surfaces than MI samples.

8. XRD patterns of PLA polymers fabricated by ISP and MI (as indicated). ISP samples exhibit a large degree of crystallinity with well-defined diffraction peaks while MI samples are essentially amorphous.

Table 1. Properties of individual materials. Standard deviations are included as errors.

	Processing Temp. (°*C*)	M_n (g/mol)	PDI	ρ (g/cm^3)	E^* (GPa) [a]	H (GPa)
TCP rods	1200	-	-	2.09	16 ± 2	0.7 ± 0.1
PCL (ISP)	60	22000	1.8	1.09	0.9 ± 0.2	0.08 ± 0.02
PCL (MI)	220	63000	1.7	1.14	1.5 ± 0.2	0.07 ± 0.02
PLA (ISP)	140	21000	2.6	1.19	6 ± 1	0.28 ± 0.09
PLA (MI)	227	71000	1.9	1.25	6.1 ± 0.6	0.27 ± 0.04

[a] *Reduced modulus,* $E^*=E/(1-\nu^2)$.

Table 2. Mechanical properties estimated from compressive tests. Standard deviations are included as errors.

	σ_0 (MPa)	m	G_{max} (MJ/m^3)	$G_{0.1}$ (MJ/m^3)
TCP	6.8 ± 0.4	3.1 ± 0.1	0.018 ± 0.07	0.07 ± 0.03
PCL-TCP (ISP)	18 ± 2	5.0 ± 0.3	0.2 ± 0.1	0.6 ± 0.2
PCL-TCP (MI)	18 ± 2	11.7 ± 0.6	0.19 ± 0.02	1.69 ± 0.09
PLA-TCP (ISP)	68 ± 7	7.2 ± 0.2	2.3 ± 0.5	5.4 ± 0.7
PLA-TCP (MI)	77 ± 19	9.0 ± 0.7	0.8 ± 0.1	3.7 ± 0.5

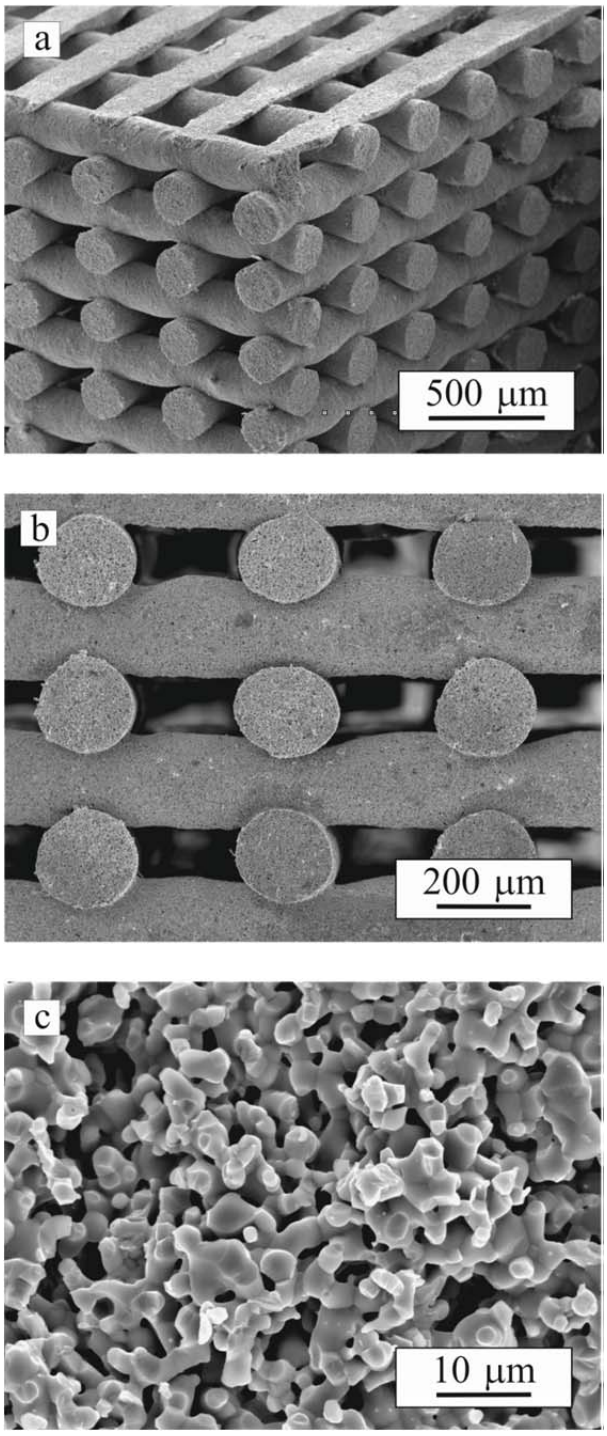

Fig.1

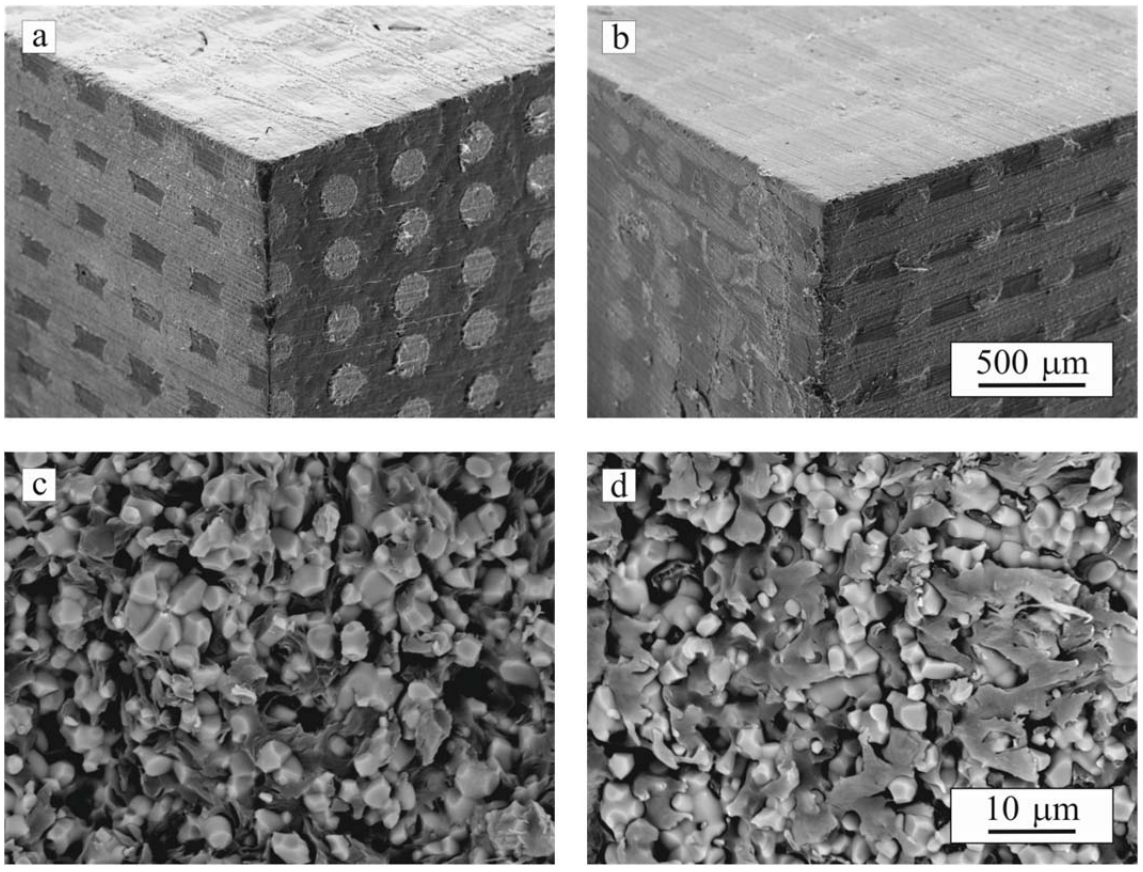

Fig.2

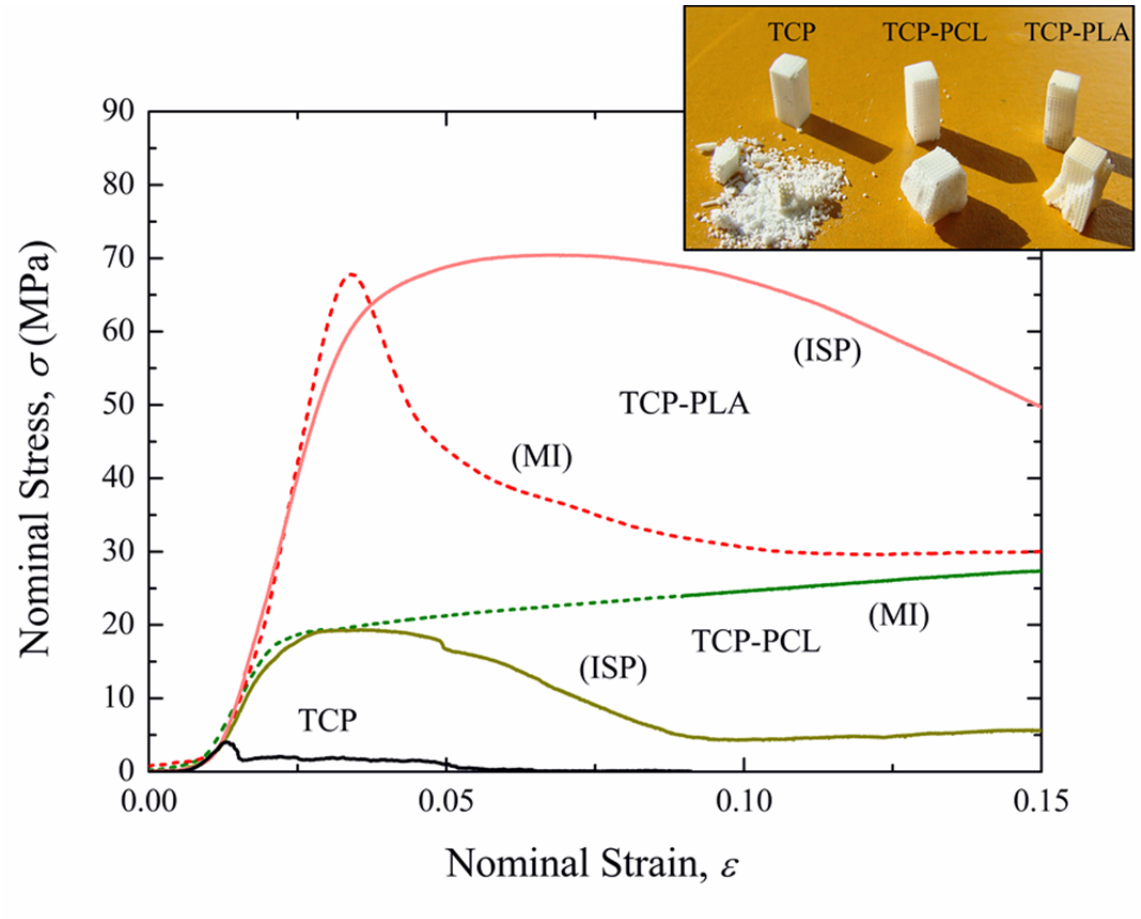
TCP
TCP-PCL
TCP-PLA
Nominal Stress, σ (MPa)
Nominal Strain, ε
0
10
20
30
40
50
60
70
80
90
0.00
0.05
0.10
0.15
(ISP)
TCP-PLA
(MI)
(MI)
TCP-PCL
(ISP)
TCP

Fig.3

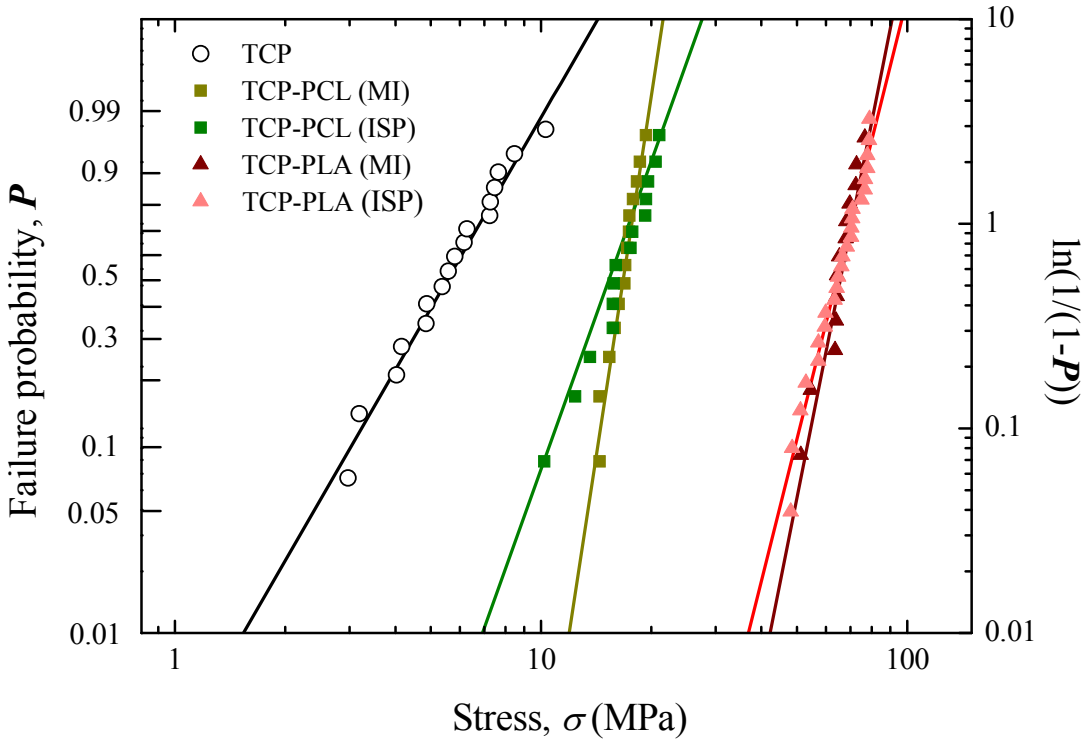
TCP
TCP-PCL (MI)
TCP-PCL (ISP)
TCP-PLA (MI)
TCP-PLA (ISP)
Failure probability, P
0.99
0.9
0.5
0.3
0.1
0.05
0.01
1
10
100
Stress, σ (MPa)
10
1
0.1
0.01
ln(1/(1-P))

Fig.4

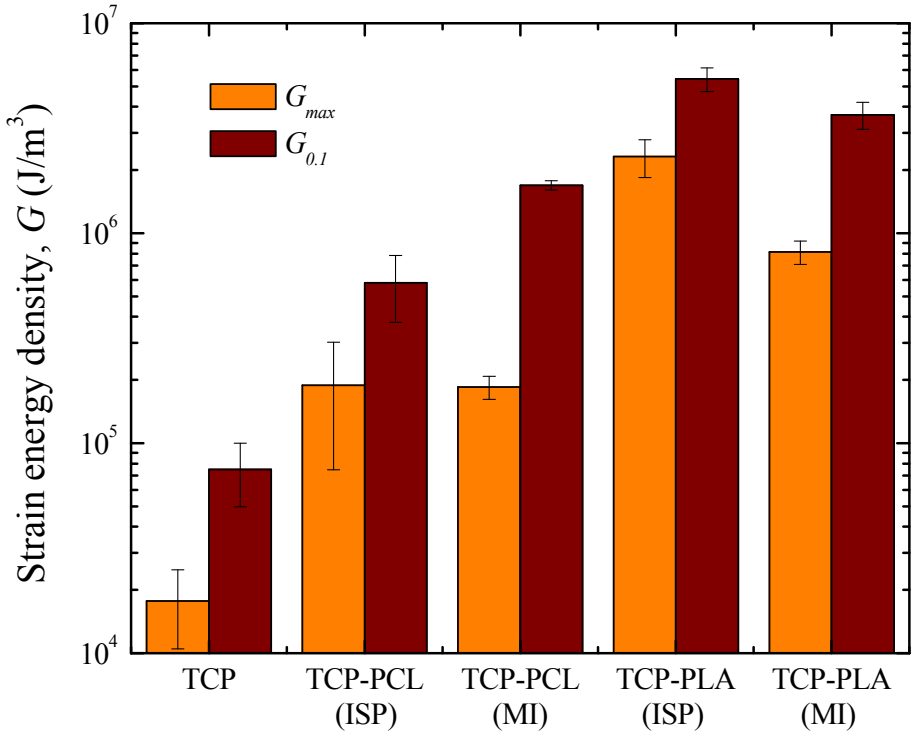
Strain energy density, G (J/m3)
10^7
10^6
10^5
10^4
G_max
G_0.1
TCP
TCP-PCL (ISP)
TCP-PCL (MI)
TCP-PLA (ISP)
TCP-PLA (MI)

Fig.5

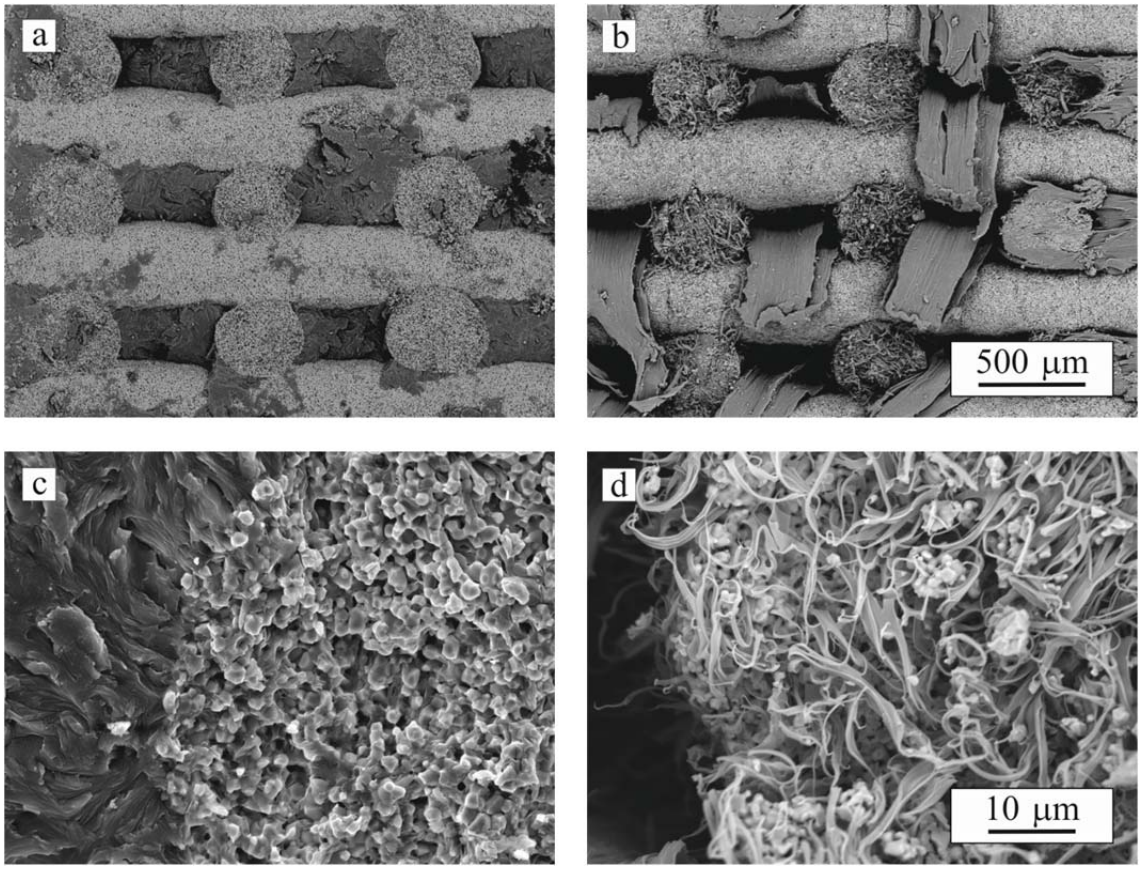

Fig.6

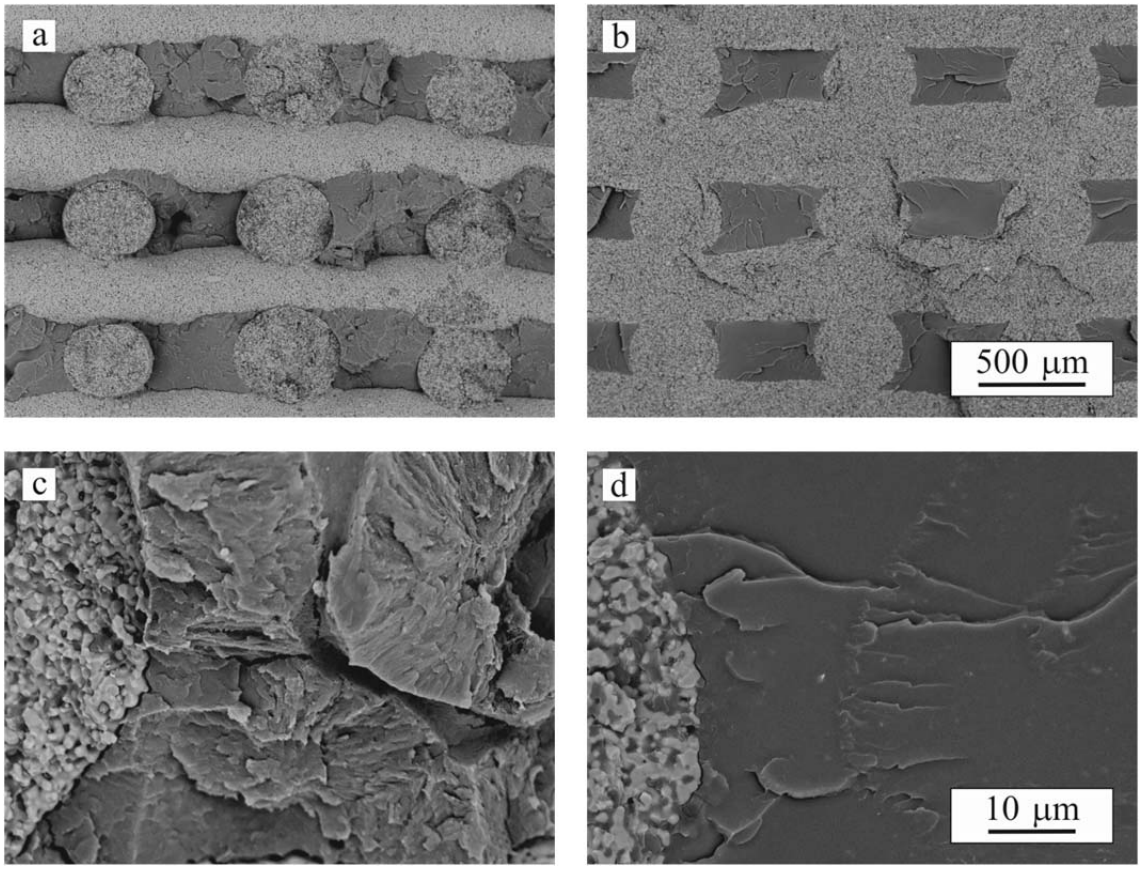

Fig.7

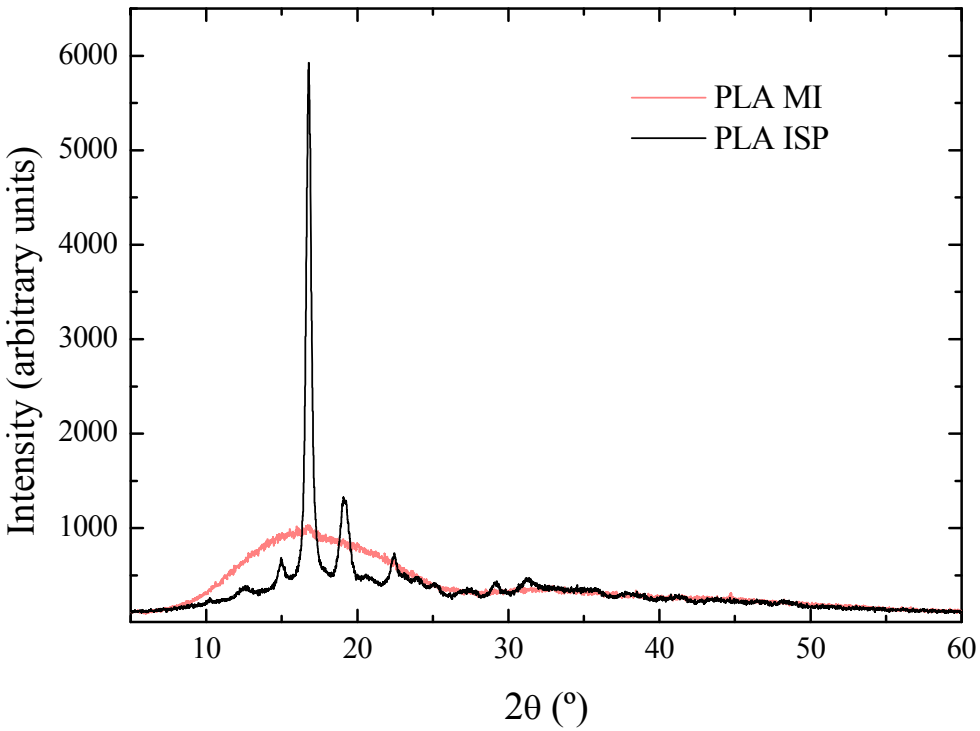
Intensity (arbitrary units)
6000
5000
4000
3000
2000
1000
10
20
30
40
50
60
2θ (°)
PLA MI
PLA ISP

Fig.8

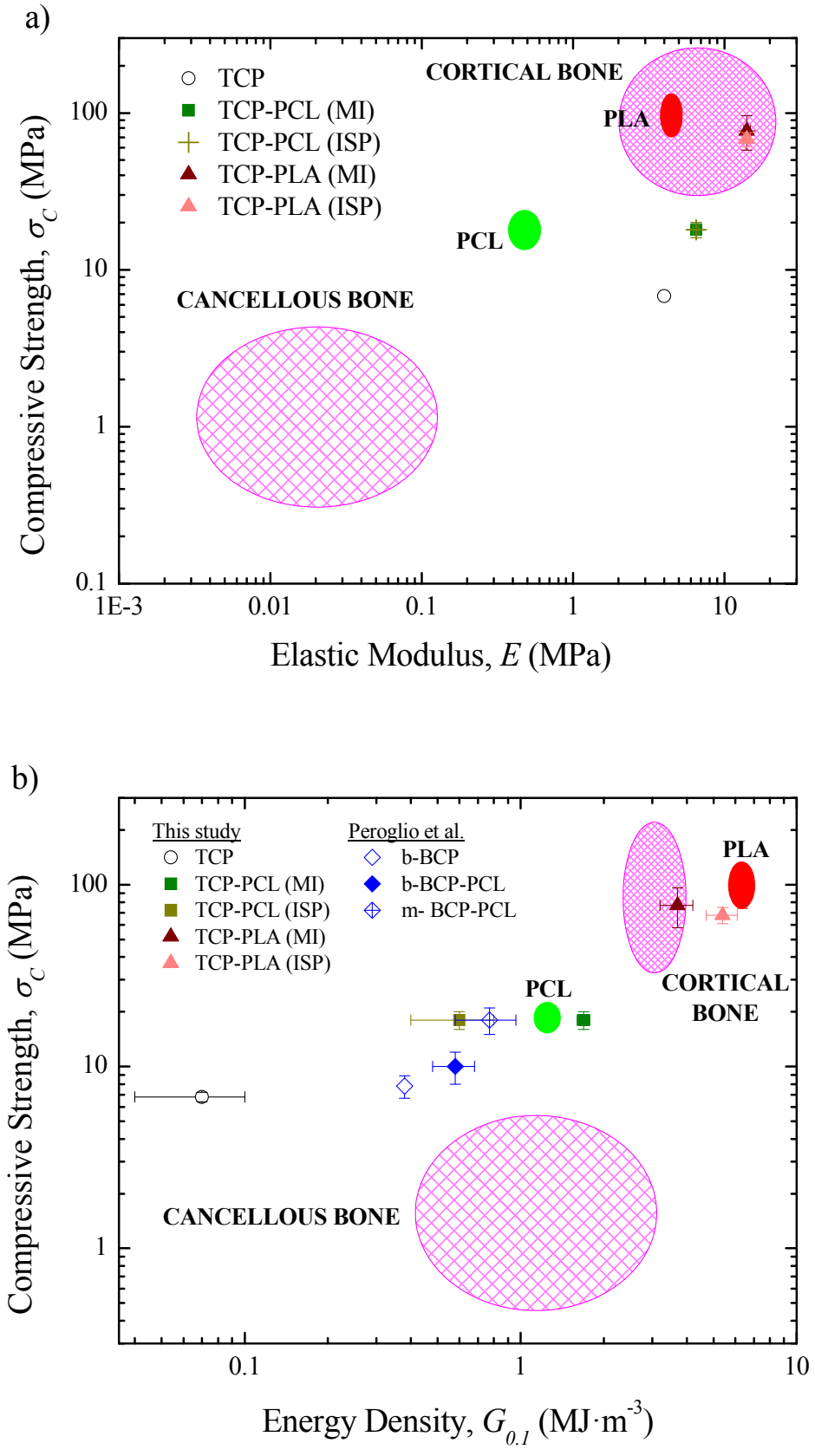
a)
TCP
TCP-PCL (MI)
TCP-PCL (ISP)
TCP-PLA (MI)
TCP-PLA (ISP)
CORTICAL BONE
PLA
PCL
CANCELLOUS BONE
Compressive Strength, σ_C (MPa)
Elastic Modulus, E (MPa)
100
10
1
0.1
1E-3
0.01
0.1
1
10
b)
This study
TCP
TCP-PCL (MI)
TCP-PCL (ISP)
TCP-PLA (MI)
TCP-PLA (ISP)
Peroglio et al.
b-BCP
b-BCP-PCL
m- BCP-PCL
PLA
PCL
CORTICAL BONE
CANCELLOUS BONE
Compressive Strength, σ_C (MPa)
Energy Density, $G_{0.1}$ (MJ·m^{-3})
100
10
1
0.1
1
10

Fig.9

Reference List

1. Nancollas GH. Formation and dissolution mechanisms of calcium phosphates in aqueous systems. In: Brown PW, Constantz B, editors. Hydroxyapatite and related materials. Boca Raton (FL): CRC Press, Inc.; 1994. p 74.

2. Miranda P, Saiz E, Gryn K, Tomsia AP. Sintering and robocasting of beta-tricalcium phosphate scaffolds for orthopaedic applications. Acta Biomater 2006;2:457-466.

3. Cesarano III J, Segalman JR, Calvert P. Robocasting provides moldless fabrication from slurry deposition. Ceram Ind 1998;148:94-102.

4. Miranda P, Pajares A, Saiz E, Tomsia AP, Guiberteau F. Mechanical properties of calcium phosphate scaffolds fabricated by robocasting. J Biomed Mater Res Part A 2008;85A:218-227.

5. Russias J, Saiz E, Deville S, Gryn K, Liu G, Nalla RK, Tomsia AP. Fabrication and in vitro characterization of three-dimensional organic/inorganic scaffolds by robocasting. J Biomed Mater Res Part A 2007;83A:434-445.

6. Peroglio M, Gremillard L, Chevalier J, Chazeau L, Gauthier C, Hamaide T. Toughening of bio-ceramics scaffolds by polymer coating. J Eur Ceram Soc 2007;27:2679-2685.

7. Peroglio M, Gremillard L, Gauthier C, Chazeau L, Verrier S, Alini M, Chevalier J. Mechanical properties and cytocompatibility of poly(epsilon-caprolactone)-infiltrated biphasic calcium phosphate scaffolds with bimodal pore distribution. Acta Biomater 2010;6:4369-4379.

8. Komlev VS, Barinov SM, Rustichelli F. Strength enhancement of porous hydroxyapatite ceramics by polymer impregnation. J Mater Sci Lett 2003;22:1215-1217.

9. Martinez-Vazquez FJ, Perera FH, Miranda P, Pajares A, Guiberteau F. Improving the compressive strength of bioceramic robocast scaffolds by polymer infiltration. Acta Biomater 2010;6:4361-4368.

10. Anseth KS, Metters AT, Bryant SJ, Martens PJ, Elisseeff JH, Bowman CN. In situ forming degradable networks and their application in tissue engineering and drug delivery. Journal of Controlled Release 2002;78:199-209.

11. Hildebrand HF, Blanchemain N, Mayer G, Chai F, Lefebvre M, Boschin F. Surface coatings for biological activation and functionalization of medical devices. Surface and Coatings Technology 2006;200:6318-6324.

12. Asmus SMF, Nakahira A, Pezzotti G. Manufacture and bioactivity of tough hydroxyapatite/nylon hybrid composites. Advanced Composite Materials 2003;11:255-264.

13. Nakahira A, Tamai M, Miki S, Pezzotti G. Fracture behavior and biocompatibility evaluation of nylon-infiltrated porous hydroxyapatite. J Mater Sci 2002;37:4425-4430.

14. Pezzotti G, Asmus SMF. Fracture behavior of hydroxyapatite/polymer interpenetrating network composites prepared by in situ polymerization process. Materials Science and Engineering: A 2001;316:231-237.

15. Pezzotti G, Asmus SMF, Ferroni LP, Miki S. In situ polymerization into porous ceramics: a novel route to tough biomimetic materials. J Mater Sci - Mater Med 2002;13:783-787.

16. Walsh D, Furuzono T, Tanaka J. Preparation of porous composite implant materials by in situ polymerization of porous apatite containing +Á-caprolactone or methyl methacrylate. Biomaterials 2001;22:1205-1212.

17. Daculsi G, Goyenvalle E, Cognet R, Aguado E, Suokas EO. Osteoconductive properties of poly(96L/4D-lactide)/beta-tricalcium phosphate in long term animal model. Biomaterials 2011;32:3166-3177.

18. Cotton NJ, Egan MJ, Brunelle JE. Composites of poly(DL-lactide-co-glycolide) and calcium carbonate: In vitro evaluation for use in orthopedic applications. J Biomed Mater Res Part A 2008;85A:195-205.

19. Hasegawa S, Ishii S, Tamura J, Furukawa T, Neo M, Matsusue Y, Shikinami Y, Okuno M, Nakamura T. A 5-7 year in vivo study of high-strength hydroxyapatite/poly(L-lactide) composite rods for the internal fixation of bone fractures. Biomaterials 2006;27:1327-1332.

20. Perera FH, Martinez-Vazquez FJ, Miranda P, Ortiz AL, Pajares A. Clarifying the effect of sintering conditions on the microstructure and mechanical properties of beta-tricalcium phosphate. Ceram Int 2010;36:1929-1935.

21. Albertsson AC, Varma IK. Recent developments in ring opening polymerization of lactones for biomedical applications. Biomacromolecules 2003;4:1466-1486.

22. de Geus M, Peeters J, Wolffs M, Hermans T, Palmans ARA, Koning CE, Heise A. Investigation of factors influencing the chemoenzymatic synthesis of block copolymers. Macromolecules 2005;38:4220-4225.

23. Kumar A, Gross RA. Candida antartica lipase B catalyzed polycaprolactone synthesis: Effects of organic media and temperature. Biomacromolecules 2000;1:133-138.

24. Miranda P, Pajares A, Guiberteau F. Finite element modeling as a tool for predicting the fracture behavior of robocast scaffolds. Acta Biomater 2008;4:1715-1724.

25. Weibull W. A statistical distribution function of wide applicability. J Appl Mech -Trans ASME 1951;18:293-297.

26. Grosvenor MP, Staniforth JN. The effect of molecular weight on the rheological and tensile properties of poly([epsilon]-caprolactone). Int J Pharm 1996;135:103-109.

27. Ramakrishna S, Mayer J, Wintermantel E, Leong KW. Biomedical applications of polymer-composite materials: a review. Compos Sci Technol 2001;61:1189-1224.

28. Hench LL. The skeletal system. In: Hench LL, Jones RJ, editors. Biomaterials, artificial organs and tissue engineering: Woodhead Publishing Limited and CRC Press LLC; 2005. p 79-89.

29. Heise A, Palmans ARA. Hydrolases in Polymer Chemistry: Chemoenzymatic Approaches to Polymeric Materials. Adv Polym Sci 2010;237:79-113.